Biosensors and Bioelectronics 35 (2012) 37–43

Contents lists available at SciVerse ScienceDirect

Biosensors and Bioelectronics

journal homepage: www.elsevier.com/locate/bios

# Piezoelectrically driven vertical cavity acoustic transducers for the convective transport and rapid detection of DNA and protein binding to DNA microarrays with SPR imaging—A parametric study

Yuka Okabe[a,1], Yulin Chen[b,1], Rishi Purohit[a], Robert M. Corn[b], Abraham P. Lee[a,c,*]

[a] Department of Biomedical Engineering, University of California-Irvine, Irvine, CA 92697, USA
[b] Department of Chemistry, University of California-Irvine, Irvine, CA 92697, USA
[c] Department of Mechanical and Aerospace Engineering, University of California-Irvine, Irvine, CA 92697, USA

ARTICLE INFO

*Article history:*
Received 23 August 2011
Received in revised form 8 December 2011
Accepted 19 January 2012
Available online 28 January 2012

*Keywords:*
Microfludics
Vertical cavity acoustic transducer
Cavitation microstreaming surface plasmon resonance imaging

ABSTRACT

Mixing within the microdomain is limited because convective mixing cannot be achieved since diffusion dominates as the main form of transport. Hence microassays can take on the order of 1 to 72 h, without the aid of a passive or active mixer to shorten the time of transport of a target molecule to a probe (Lai et al., 2004). Liu et al. (2002, 2003) developed a low cost cavitation microstreaming based mixer which is easy to implement and use, but no comprehensive study has been done to optimize such a mixer for various applications. We present a study of the effects of various frequencies and cavity parameters on mixing using dye and surface based assays with protein, DNA, and nanoparticles to obtain an optimum mixing frequency and configuration for a wide range of assay applications. We present a novel method to monitor real time binding using surface plasmon resonance imaging (SPRI) coupled with a vertical cavity acoustic transducer (VCAT) micromixer for various biomolecule surface assays. The combination of VCAT and SPRI allows assay signal saturation within one minute while conserving reagent volume. The kinetic rate constant for adsorption ($k_a$) and desorption ($k_d$) as well as the limit of detection (LOD) of 5 nM for the DNA duplex formation are reported using this VCAT micromixer.



## 1. Introduction

Lab-on-chip applications offer advantages such as low reagent consumption and enhanced surface to volume ratio, but several obstacles exist to make them practical (Henares et al., 2008). One such obstacle is the need for fast results for microassays used in point of care diagnostics. Fast results cannot be obtained due to the lack of convective mixing because diffusion dominates in the microdomain. For example, enzyme-linked immunosorbent assays (ELISA) are performed for detection and quantification of biological agents, but the process can take hours to 2 days (Lai et al., 2004; Rossier et al., 2000). In a field setting, such a time length would be impractical as results are needed quickly. The limiting factor of microassays is not the binding reaction of the biomolecule, but the mass transport of a target molecule to a probe (Lai et al., 2004; Rossier et al., 2000).

To decrease the time for microassays, several passive and active micromixers have been developed. These mixers however require bulky external equipment such as syringe pumps, are difficult to fabricate, and/or require complicated geometries (Nguyen and Wu, 2005; Stone et al., 2004; Stroock et al., 2002; Zhang et al., 2007). Liu et al. developed a micromixer based on cavitation microstreaming which is easy to assemble and use. The micromixer only requires a piezoelectric transducer which can be reused repeatedly. The micromixer consists of cavity acoustic transducers (CATs) that are placed inside a chamber or channel, which trap air when a fluid is flowed over the cavities. CATs have been shown to be useful for various applications such as pumping (Tovar and Lee, 2009), cell lysis (Marmottant and Hilgenfeldt, 2003), and mixing (Ahmed et al., 2009; Liu et al., 2003, 2002). CATs can be placed laterally (LCAT or lateral cavity acoustic transducer) or vertically (VCAT or vertical cavity acoustic transducer) within a channel or chamber depending on the application. Cavitation microstreaming occurs when an air bubble undergoes oscillations in a fluid, creating velocity and pressure fluctuations in the surrounding fluid (Fig. 1) (Tho et al., 2007). The air–liquid interface acts like a vibrating membrane which pushes fluid around the interface when the air bubble is subjected to a sound field. The frequency and the amplitude of the sound field affect the mode of oscillation of the air–liquid interface which affects the streaming near the bubble (Elder, 1959; Tho et al., 2007). Liu et al. utilized cavitation microstreaming with trapped

* Corresponding author at: 3130 Engineering Hall, Irvine, CA 92697, USA.
*E-mail addresses:* aplee@uci.edu, yokabe@uci.edu (A.P. Lee).
[1] These authors contributed equally to this work.

0956-5663/$ – see front matter © 2012 Elsevier B.V. All rights reserved.
doi:10.1016/j.bios.2012.01.028

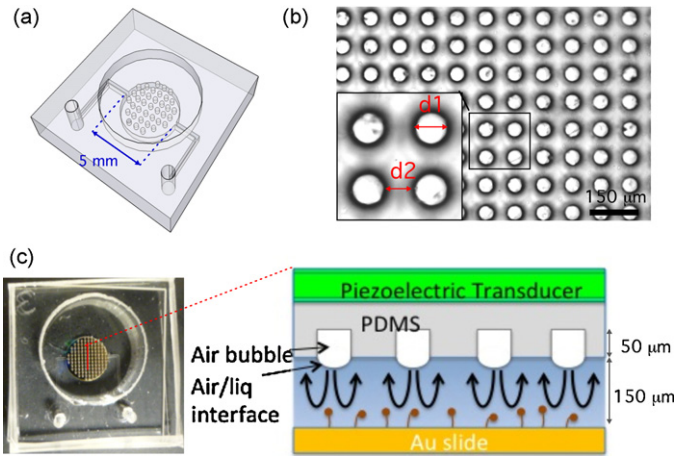


**Fig. 1.** (a) A schematic representation of VCAT micromixer used for SPRI measurements. (b) A microscope image of the top view of the cavities in the devices. d1 indicates the cavity diameter and d2 indicates the edge-to-edge spacing between the cavities. (c) VCAT micromixer device bonded to Au slide spotted with ssDNA. Cross-sectional schematic shows cavitation microstreaming which occurs when an air liquid interface is excited due to a piezoelectric transducer.

air bubbles in cavities to achieve mixing with flow rates of 5 mm/s, but only excited the air bubbles at one frequency (5 kHz) (Liu et al., 2002). Liu demonstrated with dye as well as with immunomagnetic cell capture using *Escherichia coli* the feasibility of CAT mixing, but the cell capture experiment was run for 30 min (Liu et al., 2002) and the DNA hybridization experiment showed signal saturation after 40 min (Liu et al., 2003). Both studies showed the use of the micromixer in biological applications, but have not shown the speed enhancement possible with an optimized micromixer or how quickly signal acquisition can truly be obtained. Furthermore, Liu's usage of polycarbonate and a milling machine to fabricate the CATs limited the size of the cavities and its possible application in microdevices (Liu et al., 2003, 2002). With the use of standard photolithography, a precise array of CATs can be created anywhere on the microdevice that would not be possible with the use of a miller. Huang et al. developed a millisecond micromixer which placed a CAT in the middle of a channel. Huang's mixer only utilized one bubble within a channel at a certain frequency and demonstrated mixing using dye and water only with no biological application shown (Ahmed et al., 2009). No thorough study of the effects of frequency or the size and spacing of the air cavities has been conducted yet on mixing efficiency and speed enhancement for different types of assays.

Surface plasmon resonance imaging (SPRI) is an excellent alternative to traditional fluorescence-based measurements (Hickel et al., 1989; Rothenhausler and Knoll, 1988; Yeatman and Ash, 1987). SPRI is a surface-sensitive optical technique that detects the changes in the local refraction index upon binding (Rossier et al., 2000), which is a significant advantage in biological samples as it offers label-free detection without the need for on-site processing (e.g. labeling and enrichment) (Lee et al., 2006; Phillips et al., 2006; Shumaker-Parry and Campbell, 2004; Wolf et al., 2005). In addition, SPR-based detection methods are capable of the urgent need for inexpensive, portable sensors which are able to rapidly and sensitively detect agents, and it has evolved into a primary method for the bioaffinity measurements for DNA, RNA, DNA-binding proteins, and biomarkers onto DNA microarrays (Chen et al., 2009; Reuter et al., 1999; Wegner et al., 2004). This technique also led to applications for a variety of biological detection such as DNA diagnostics and genotyping, gene expression analysis, and point-of-care testing (POCT) (Carrascosa et al., 2009; Feriotto et al., 2001; Nilsson et al., 1997).

In this paper, we describe our efforts to combine the concepts of DNA microarrays using SPRI detection method with a VCAT micromixer. Renaudin et al. combined SPR with surface acoustic waves (SAW) to increase the time of mass transport of an avidin-biotin assay 5 times. However saturation of signal takes 20–30 min with the SAW mixer integrated on a common substrate with SPR which is still considerably a long time to obtain a signal compared to our system (Renaudin et al., 2010). The green dye mixing is initially conducted to find the optimum mixing frequency and VCAT configuration for the surface assays. The SPRI measurements demonstrate that the VCATs microdevice enhanced the mass transport efficiency for single-stranded DNA (ssDNA), single-stranded binding protein (SSB), DNA-modified gold nanoparticles (AuNPs) to DNA sequence by more than a hundred times, making this faster compared to the diffusion cases. The VCAT micromixer paired with SPRI gives a saturation of signal within a minute which is considerably faster compared to other mixers and detection systems.

## 2. Materials and methods

### 2.1. Materials

11-Amino-1-undecanethiol hydrochloride (MUAM; Dojindo), poly-L-glutamic acid (MW = 2000–15,000; pGlu; Sigma), 1-ethyl-3-(3-(dimethylamino) propyl) carbodiimide hydrochloride (EDC; Pierce), N-hydroxysulfosuccinimide (NHSS; Pierce), ethanol (Gold Shield, absolute) and urea (Sigma–Aldrich), polydimethylsiloxane (PDMS) curing agent and prepolymer (Sylgard 184, Dow Corning), were used as received. The DNA sequences used in this paper are summarized in Table 1. All DNA sequences were checked using mfold DNA folding calculations and showed no hairpin formation (developed by M. Zuker) (Zuker, 2003). A PBS buffer (100 mM $Na_2HPO_4$, 0.3 M NaCl, 5 mM $MgCl_2$, 1 mM EDTA, adjusted to pH 7.4) was used for all DNA fabrication and hybridization.

### 2.2. Microfluidic device fabrication

Standard soft lithography was utilized to fabricate the devices (Duffy et al., 1998). The master mold fabrication consisted of a two-step SU-8 process. SU-8 100 was spun on a silicon wafer as the first step to create the chambers and the channels of the device. For the second step, SU-8 50 was spun on the wafer to create the posts for the air cavities. The mold was then developed using standard SU-8 procedures. PDMS was poured onto the mold and allowed to cure overnight. A thick connective PDMS layer was then plasma bonded onto the PDMS cured onto the mold. The two-layer PDMS device was then peeled off the mold and plasma bonded using air plasma onto a glass slide after the inlet and the outlet are created. All devices have a chamber and channel height of 150 μm and 50 μm deep cavities, respectively. The schematic representation of the VCAT device is shown in Fig. 1(a). Fig. 1(b) is a microscope image of the top view of the cavities in the devices, where d1 indicates the cavity diameter and d2 indicates the edge-to-edge spacing between the cavities.

**Table 1**
Single strand DNA sequences for SPRI measurements.

| Symbol | Sequence |
|---|---|
| D1 | 5′-$(A)_{30}$-$(CH_2)_6$-$NH_2$-3′ |
| cD1 | 5′-$(T)_{30}$-3′ |
| D2 | 5′-TTC GGT TCG TGC TTA TGT GTC TGG ATT TCG-$(CH_2)_6$-$NH_2$-3′ |
| cD2 | 5′-CGA AAT CCA GAC ACA TAA GCA CGA ACC GAA-$(CH_2)_6$-SH-3′ |
| D3 | 5′-$(T)_{30}$-$(CH_2)_6$-$NH_2$-3′ |

### 2.3. Green dye mixing experiments

Green dye was flowed into inlet 1 at 1 μL/min while water was flowed into inlet 2 at 5 μL/min using a syringe pump (Harvard Apparatus PicoPlus) (Fig. 1, supporting matieral). The piezoelectric transducer was placed over the air cavities after Aquasonic 100 ultrasound gel was placed between the PDMS device and the piezoelectric transducer to ensure there is minimal loss of signal transmission. Lead wires from the piezoelectric transducer were connected to a function generator (Agilent 33220A). The function generator is programmed to output a square wave at various frequencies in the 1–40 kHz range with a fixed voltage of 10 $V_{pp}$.

A video of mixing with 1 s of non-mixing followed by 4 s of mixing was taken using a DSLR camera (Canon Rebel) and hypercam program. ImageJ was used to measure the average pixel intensity of the area of mixing as well as the green dye area. Each video was normalized using the equation

$$E_{mix} = \frac{I_g - I_i}{I_o - I_g} + 1$$

where $I_g$ is the green dye area pixel value, $I_i$ is the pixel value of the current frame, and $I_o$ is the initial area pixel value where mixing will take place (Fig. 1, supporting material). When $E_{mix}$ reaches the value of 1, it will indicate complete mixing of the chamber while a 0 indicates no mixing. The configurations tested using green dye were 50 μm, 100 μm, and 200 μm in diameter cavities (d1) spaced half (d1/2) original (d1) and double (2*d1) the cavity size from the edge of one cavity to the edge of another (d2). We varied the diameter and the spacing of the cavities, which are d1 and d2 μm, respectively, and also the driving frequency for the piezoelectric transducer to obtain an optimized condition for mixing efficiency.

### 2.4. Preparation of ssDNA-modified gold nanoparticles (AuNPs)

A standard citrate reduction Turkevich method (Turkevich et al., 1951) was used to synthesize AuNP solutions with a $\lambda_{max}$ of 520 nm and an average particle diameter of approximately 13 nm. The AuNPs solution has an extinction coefficient of $2 \times 10^8\ M^{-1}\ cm^{-1}$. DNA-modified AuNPs were then prepared as follows (Lee et al., 2008; Sendroiu and Corn, 2008): 10 μL of 1 mM 3′-thiol-modified DNA (cD1 or cD2) was added to 1 mL of Au nanoparticle stock solution (~15 nM) and kept at 37 °C overnight. 500 μL of phosphate buffer (0.3 M NaCl, 30 mM phosphate, pH 7.4) was subsequently added to the solution and kept at 37 °C. The excess DNA was removed by centrifuging the nanoparticle solution at 12,000 rpm for 30 min and removing the supernatant. The AuNPs were resuspended in PBS buffer (pH 7.4). This washing step was repeated three times.

### 2.5. SPRI chip and DNA microarray fabrication

SPRI chips were fabricated using a metal mask to vapor deposit (Denton DV-502A) a 45-nm gold film with a 1-nm underlayer of chromium on top of SF-10 glass slides. Two kinds of metal mask were used: a diameter of 5-mm big gold circle spot (for lateral mixing measurements) or 16 small gold spots (1 mm diameter each, for microarray measurements). Amine-terminated ssDNA was attached to the gold array spots with the DNA surface attachment chemistry described elsewhere (Chen et al., 2009). Briefly, the slides were immersed in a 1 mM ethanolic MUAM solution for at least 12 h. After rinsing with ethanol and water then drying with nitrogen gas, 400 μL pGlu (3 mg/mL) in PBS buffer was applied onto each slide to form pGlu monolayer onto the amino-terminated MUAM. PGlu is first electrostatically adsorbed onto an amine-terminated monolayer (MUAM), and then a carbodiimide coupling reaction simultaneously binds pGlu to the surface and attaches amine-modified DNA onto the pGlu monolayer. This two-step process provides ample space and additional flexibility to the surface-attached ssDNA for hybridization and protein binding. For 5 mm diameter gold circle spot, 10 μL of 250 μM amine-terminated ssDNA solution was exposed to the slide. For 1 mm diameter gold-spot array, 0.45 μL of a 250 μM amine-terminated ssDNA solution was applied on each spot. The slides were rinsed with water and dried by nitrogen gas prior to use.

### 2.6. SPRI measurements

SPRI measurements of differential reflectivity images ($\Delta\%R$) at 830 nm were obtained using an SPRimager instrument (GWC Technologies) as described previously (Chen et al., 2009; Nelson et al., 2000). All SPRI measurements were performed using the VCAT micromixer with 100 μm diameter air cavities spaced 50 μm edge to edge with a height of 50 μm as shown in Fig. 1(b) and (c). The piezoelectric transducer was attached at the top of the device with ultrasound gel in between. The microfluidic chamber was loaded with 10 μL of buffer solution and the piezoelectric transducer was turned on to allow a base measurement of the surface before the solution of interest was injected into the chamber. In Fig. 1(c), cross-sectional schematic shows cavitation microstreaming which occurs when an air liquid interface is excited due to a piezoelectric transducer. In the lateral mixing measurements, 1.8 μL of concentrated analyte was then injected into the chamber so as not to saturate the chamber with the initial injection step and the binding was tracked for the duration of the assay. In the microarray binding assay, 5 μL of low-concentration analytes were injected into the chamber. The piezoelectric transducer was actuated at 32 kHz and at 2 $V_{pp}$ amplified to 20 $V_{pp}$ through the voltage amplifier.

## 3. Results and discussions

### 3.1. Green dye results

To identify the optimal frequency for mixing, the resonant frequencies of the various bubble sizes were calculated using Minnaert's equation:

$$f = \frac{1}{2\pi a}\sqrt{\frac{3\gamma P_o}{\rho}}$$

where $a$ is the radius of the bubble, γ is the ratio of specific heats for the gas, and $P_o$ is the hydrostatic pressure, and ρ is the density of the liquid (Liu et al., 2002). According to Minnaert's equation, the resonant frequencies of the bubbles for 50 μm, 100 μm, and 200 μm are 130 kHz, 65 kHz, and 32 kHz, respectively. However, the VCATs do not cause strong mixing until frequencies in the range of 30–40 kHz are reached (Table 1, supporting material). Frequencies outside this range cause little to no mixing within the chamber even upto frequencies of 200 kHz. Therefore an empirical approach of using green dye mixing was used to identify the best mixing frequency for the whole system due to the resonant frequency of the bubbles not causing adequate mixing. The configuration with the greatest mixing efficiency is 100 μm cavity spaced 100 μm apart at 34 kHz.

The mixing efficiency is greatest for cavity diameter to spacing ratio of 1 (Fig. 2, supporting material). Out of the nine configurations, the greatest mixing efficiency occurs with the 100 μm diameter cavity spaced 100 μm apart, the 200 μm diameter cavity spaced 200 μm apart, and the 50 μm diameter cavity spaced 50 μm apart respectively (Fig. 2, supporting material). The ratio of 0.5 is the next best mixing efficiency followed by a ratio of 2. The closer the bubbles are in relation to one another, the streaming patterns can couple leading to better mixing within the chamber. The ratio of

2 has relatively the lowest mixing efficiency out of the three ratios due to the bubbles being too far apart for the streaming patterns to effectively couple. However, the ratio of 0.5 is probably lower than that of 1 due to the coupling of the flows having an optimum ratio. The ratios of 0.5 and 2 for all three cavity sizes are similar in value while the ratio of 1 produces the best mixing.

The bubble size has an effect on the mixing efficiency with bubble diameter of 100 μm giving the best mixing efficiency followed by 50 μm and then 200 μm (Fig. 3a–c, supporting material). The mixing efficiency increase from the 50 μm bubble to the 100 μm bubble is due to the amplitude differences from the liquid-gas interface of the bubble as larger bubbles cause increased microstreaming. The 200 μm bubble, although larger than the 100 μm bubble, does not produce better mixing due to a lack of stability. The 100 μm and 50 μm bubbles when excited at higher voltages (data not shown) stay relatively intact within the cavities while for the 200 μm cavity, the bubble will pop out of the cavity or the air–liquid interface changes shape. The lack of bubbles or different shapes the bubble would take in the cavity leads to an insufficient coupling of the streaming patterns, thus leading to a lower mixing efficiency.

Using the results from green dye mixing, the optimum frequency for mixing is obtained for certain configurations of cavity size and spacing for a given channel height. All the SPRI measurements in the following paragraphs were performed using 32 kHz mixing frequency, and with devices of cavity size of 100 μm diameter with 50 μm spacing. Although the 100 μm diameter cavity with 100 μm spacing at 34 kHz produced the best mixing efficiency, the results from assays using SPRI shows inadequate uniform mixing. Spotting occurs on the surface looking at the difference images of SPRI which would not be optimal for surface assays (Fig. 4, supporting material). The possible reason might be that the mixing is too strong and interferes with the biomolecule binding at certain areas on the surface. Therefore the next best efficiency ratio of 0.5 was used for several different biomolecule surface assays to determine the improvement that VCAT mixing has on signal intensity and time of assay with SPRI.

### 3.2. SPRI real time measurements of lateral mixing

To quantify the mixing efficiency of the VCAT micromixer, a set of SPRI measurements were performed to determine the fidelity of DNA hybridization adsorption and SSB adsorption onto these ssDNA monolayers (Fig. 5, supporting material). In the lateral mixing measurements, a high concentration of analytes are applied to the surface to ensure a clear signal without noise and to study the mass transport limitations of using the VCAT micromixer. Different biomolecules with different diffusion coefficients were tested to see if VCAT mixing can be applied to various applications. VCAT mixing was utilized to see the three kinds of real time binding enhancement for surface assays for ssDNA to ssDNA, protein to ssDNA, and ssDNA-modified gold nanoparticle (AuNP) to ssDNA (Fig. 6, supporting material). The ssDNA attachment chemistry onto the gold surface (5 mm diameter circle spot) is the same procedure that we have used in previous papers (Chen et al., 2009).

For the following lateral mixing experiments, surface probe D1 was immobilized on the gold surface, and the real time binding data was obtained by SPRI (schematically shown in Fig. 2(a)). The vertical diffusion barrier can be neglected since the height of the PDMS chamber is 150 μm, and it will only take one minute to diffuse from the top of the chamber to the bottom (He et al., 2000; Lukacs et al., 2000; Rudyak et al., 2008). Therefore we will be more interested in the lateral mixing efficiency of this device. In order to understand the lateral mixing, 1.8 μL of concentrated reactant (1 mM of ssDNA, 1.3 μM of SSB, and 0.1 μM of AuNP) was injected in the chamber and the real time binding was measured using SPRI. The reactant only filled the inlet channel and stopped within the region marked with the blue triangle marker in Fig. 2(b). The progression of mixing is shown in Fig. 2(c) taken by the real-time monitoring of SPRI. Two cases were conducted for each biomolecule of interest: diffusion based assay and VCAT mixing based assay. For the diffusion based assay, the piezoelectric transducer was attached on the device but not turned on; the biomolecules diffused and were driven by Brownian motion and a concentration gradient. For the VCAT mixing based assay, the piezoelectric transducer was

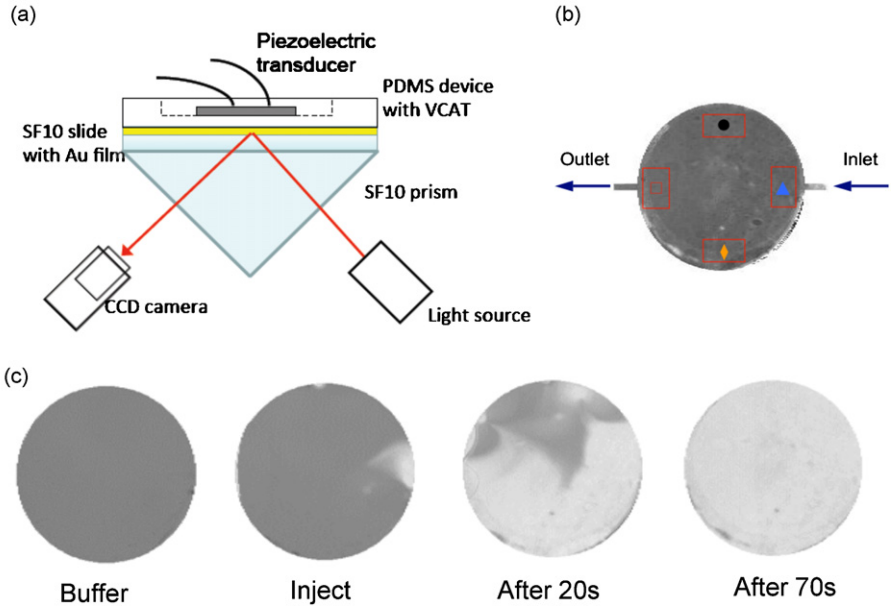


**Fig. 2.** SPRI measurements (a) Schematic apparatus for SPRI. (b) Areas tracked real-time with SPRI. The inlet region where the reactant is injected is marked with (▲). The chamber is placed vertically with the top of the chamber (●) and the bottom (◆). (c) SPRI images of mixing occurring in real time. After 70 s, the chamber is uniformly mixed and binding has taken place for the assay. Note that this is taken from a binding experiment of SSB to ssDNA. White color indicates the change in reflectivity caused by binding.

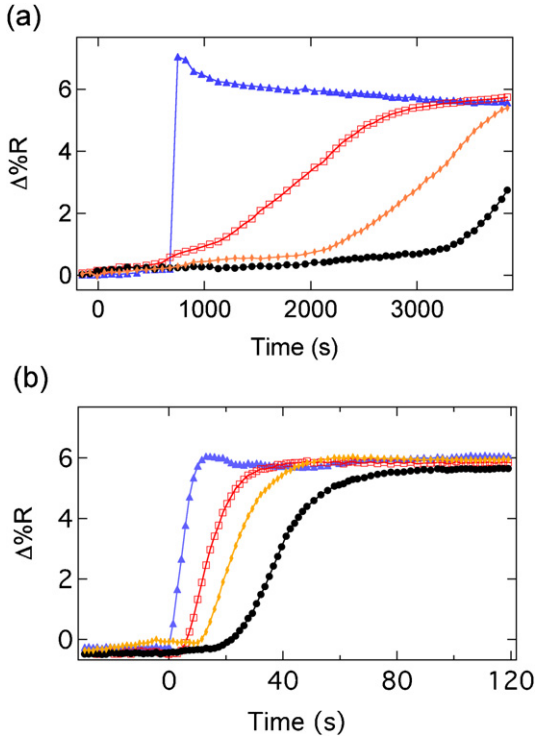


**Fig. 3.** Real-time binding measurement of DNA–DNA hybridization adsorption by SPRI measurements. 1.8 μL of concentrated 1 mM cD1 injected in the chamber and real time binding shown (a) without VCAT mixer and (b) with VCAT mixer. The reactant only filled the inlet channel and stopped within the region marked with the blue triangle marker in Fig. 2(b). The colors with different marker represents the region of interest in Fig. 2(b). Δ%*R* indicates change in reflectivity. (For interpretation of the references to color in this figure legend, the reader is referred to the web version of the article.)

turned on during the whole injection and binding procedure. The real time binding data was recorded from the diffusion based assay and compared to VCATs mixing based assay.

### 3.3. DNA to DNA

Amine-modified DNA, D1, was attached onto the pGlu monolayer using the surface chemistry described above, and the complementary DNA to D1 (denoted as cD1) was injected into the mixing chamber and the binding of cD1 to the surface probes D1 was tracked in real time. Note that all the DNA sequences are listed in Table 1. Binding real time measurement of diffusion based assay without VCAT amplification is shown in Fig. 3(a), and it depicts that after more than an hour, the complementary DNA (cD1) distributes unevenly close to the injected inlet. Compared to the VCAT assay, binding saturation with the optimum mixing frequency is within a minute (as shown in Figs. 2c and 3b). The binding efficiency shows more than a hundred times increase in speed than without the VCATs.

### 3.4. SSB protein to DNA

A series of similar experiments were performed to determine whether VCATs can enhance the transportation of larger molecules, such as proteins or nanoparticles after having confirmed that VCATs did enhance the transport of ssDNA to hybridize onto ssDNA monolayers. SSB protein was injected into the mixing chamber to bind to the surface probe D1 and tracked over time. To see the difference of the effect of using a non-optimal mixing frequency, an assay was done at 2 kHz as well as 32 kHz (Fig. 7, supporting material). At 2 kHz, binding saturation takes considerably longer than at 32 kHz to become uniformly mixed. Compared with the 32 kHz, the 2 kHz takes approximately 12 min for the whole chamber to be uniformly mixed while for 32 kHz, the chamber is uniformly mixed within a minute. The frequency at which the bubbles are excited plays a huge role in determining how long mixing and signal acquisition takes. The use of the optimal frequency results in a 10-fold increase in the mixing efficiency leading to a shorter time for assay completion. However, even at the non-optimal frequency, the mixing seen for 2 kHz is considerably faster than relying on passive diffusion which can take upwards of 30 h for the biomolecule of interest to travel the diameter of the chamber and reach surface probes on the other side of the chamber (Fig. 7, supporting material).

### 3.5. Gold nanoparticle to DNA

ssDNA cD1 modified gold nanoparticles (denoted as cD1-AuNPs) were injected into the mixing chamber to bind to the surface probe D1 and tracked over time. Similar real time binding data is shown in Fig. 8, supporting material. Compared to SSB and ssDNA, AuNPs have a larger diffusion coefficient leading to a longer time for transport (He et al., 2000; Lukacs et al., 2000; Rudyak et al., 2008). Calculated diffusion time for AuNPs is ten to hundreds times longer than for SSB and ssDNA, respectively, to travel the diameter of the chamber. The diffusion data obtained without VCAT mixing shows that areas farther away from the inlet and at the top of the chamber do not reach binding saturation after 30 min. Compared with SSB and ssDNA diffusion data, the same areas have considerably less binding in the same amount of time due to the size difference of AuNP. With the VCATs, binding saturation for the whole 5 mm chamber is reached within a minute for AuNPs which is comparable to the time for binding saturation of SSB and ssDNA even though AuNP has a larger diffusion coefficient. The VCAT is able to uniformly mix large as well as small biomolecules equally, making it desirable for various applications.

To ensure that the signal from the binding is not due to nonspecific binding of the above biomolecules, a ssDNA sequence which is noncomplementary to those pipetted on the surface was tested. 1.8 μL of 1 mM noncomplement poly(A)$_{30}$ DNA was injected into the chamber and was tracked over time. The signal from the noncomplementary DNA is low even after mixing for 10 min (Fig. 9, supporting material). In cases of high ligand density and a flow cell with low flow, the VCAT micromixer can be utilized to overcome the mass transport limitation of analyte depletion near the ligand surface. The VCAT micromixer can replenish the depletion layer by uniformly mixing the sample volume to bring the target analyte to the surface faster than diffusion or in low flow (laminar flow) cases. The calculated diffusion times for ssDNA, SSB, and AuNP are estimated as 60 s, 90 s, and 380 s, respectively (Frietas, 2003; Nkodo et al., 2001), to travel the chamber height according to the equation $t = L^2/4D$, where $t$ is time of diffusion, $L$ is the travel distance, and $D$ is the diffusion coefficient. Looking at DNA to DNA, SSB to DNA, and AuNP to DNA binding, binding saturation is achieved within a minute for the whole chamber which is faster than the time of diffusion of an analyte traveling the height of the chamber to replenish the depletion layer.

### 3.6. Microarray binding

To show the feasibility of the VCAT micromixer for microarrays with various probes as with an actual application to detect multiple markers, a slide was prepared with three different DNA sequences to bind DNA, SSB, and AuNP. To overcome diffusion problems especially regarding large molecules such as proteins or nanoparticles, a flow through system is usually required for detection on microarrays (Halpern et al., 2011; Wark, 2008). However, a larger volume of reagent (around 500 μL) is needed for a flow through system.

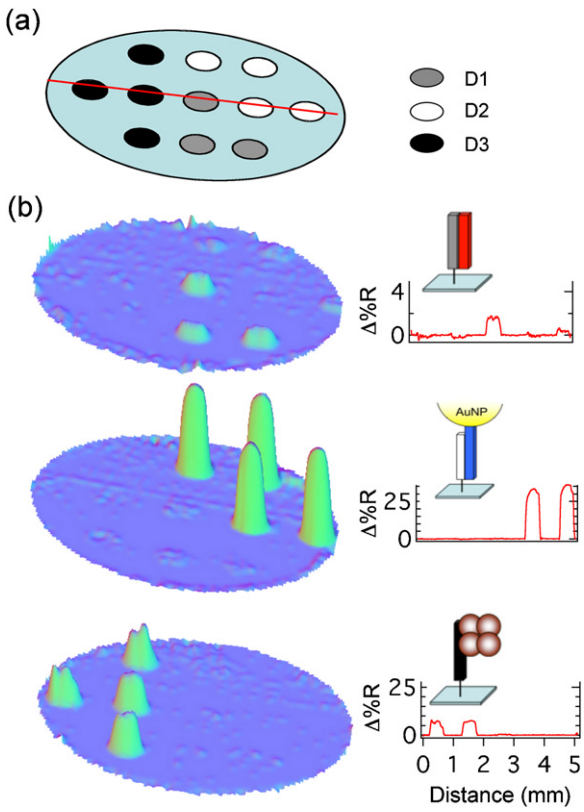


**Fig. 4.** SPRI measurements for microarray using the VCAT mixer. (a) Representation of three-component DNA probe microarray (D1, D2, D3) for ssDNA, Au-NP, and SSB respectively, including the location of the line profile. (b) SPRI difference images obtained by substracting images acquired before and after the biomolecule flowing step (cD1, cD2-AuNPs, and SSB subsequently). Three line profiles are taken from the SPRI difference images for each biomolecule.

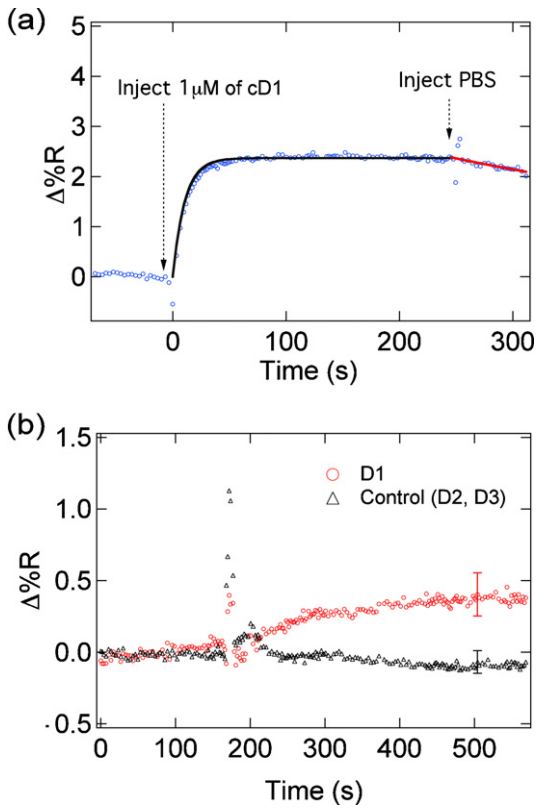


**Fig. 5.** (a) Real time binding data of low concentration of ssDNA to ssDNA (1 μM cD1). cD1 is injected into the chamber at time 0 and PBS buffer is injected at time 250 s. The real time binding data is fitted with kinetic equations (1) and (2) to obtain $k_a$ and $k_d$ values of $9.18 \pm 2.45 \times 10^4\ M^{-1}\ s^{-1}$ and $1.95 \pm 0.85 \times 10^{-3}\ s^{-1}$, respectively. (b) Real time binding data of 5 nM ssDNA. cD1 is injected into the chamber and signal is seen from D1, but no signal from D2 and D3 indicating that the signal is not due to noise. The data points are the average values from different array spots, and the error bars represent the standard deviation of these measurements.

In this part, the three-element microarray was created by spotting solutions containing different sequences ssDNA (D1, D2, and D3 in Fig. 4(a)) on the surface, and then sequentially exposing to complementary ssDNA cD1, cD2 modified AuNPs (cD2-AuNPs), and then SSB. A 5 μL solution of each binding reactant (1 μM of cD1, 2 nM of cD2-AuNPs, 10 nM of SSB) was injected to fill the whole chamber while the VCAT mixer was turned on. The chamber is subsequently washed out and the next analyte is flowed into the chamber and allowed to bind with its corresponding probe with the VCAT mixer turned on. SPRI difference images were obtained by subtracting the pixel intensity of the image obtained before the analyte was flowed in from the image obtained after the analyte was in the chamber. The line profiles after each binding are shown in Fig. 4(b). When cD1 is flowed into the chamber, the spots with DNA probe D1 show a signal while the other spots with D2 and D3 DNA probe show no signal. Nonspecific binding did not occur nor did the bound biomolecule detach from the surface during the loading and washing steps for each biomolecule with the VCATs on. The VCAT mixer can be used for microarrays with a small volume of reagent as compared to a flow through system while still overcoming diffusion.

### 3.7. Kinetic measurement and detection limit for ssDNA hybridization

Kinetic measurements of the VCAT micromixer are performed on the microarray slides described above, which are immobilized with three ssDNA sequences: D1, D2, and D3. A 1 μM ssDNA solution, cD1, which is complementary to D1 is applied onto the slide. A two-state model is assumed (i.e. A + B ↔ AB) for hybridization kinetics to obtain the rate constant of adsorption ($k_a$) and desorption ($k_d$) for DNA hybridization by fitting the kinetic equations (Eq. (1) & (2) below). In terms of SPR response ($\Delta\%R$), the desorption process which is independent of the flow-in cD1 concentration can be expressed as,

$$\Delta\%R(t) = \Delta R e^{-k_d(t-t_0)} \quad (1)$$

where $\Delta R$ corresponds to the SPR signal change at $t_0$. For the adsorption process,

$$\Delta\%R(t) = \frac{k_a C \Delta R_{max}}{k_a C + k_d}[1 - e^{-(k_a C + k_d)t}] \quad (2)$$

where $C$ is the applied solution concentration (cD1) and $\Delta R_{max}$ refers to the maximum SPR signal obtained when all surface binding sites are occupied. The $k_a$ and $k_d$ of a 30-mer DNA hybridization using VCAT micromixer are $9.18(\pm 2.45) \times 10^4\ M^{-1}\ s^{-1}$ and $1.95(\pm 0.85) \times 10^{-3}\ s^{-1}$, respectively. The error bars represent the standard deviation of three independent repeated measurements. Fig. 5(a) shows the real-time data together with the fitted lines. The desorption equilibrium constant $K_D$ ($=k_d/k_a$) is $2.12(\pm 0.80) \times 10^{-8}$ M, which is comparable with Jensen et al. (1997). The values of $k_a$ and $k_d$ from VCAT micromixer are slightly larger than normal flow-cell system (as shown in Fig. 10, supporting material) while $K_D$ is at the same order of those reported data (Jensen et al., 1997), indicating the device does increase the kinetic process for both adsorption and desorption, but leaving equilibrium condition similar to a flow-cell system.

In Fig. 5(b), detection limits of 5 nM DNA–DNA binding are obtained from VCAT micromixer coupled with SPRI, which show

good commitment to other conventional SPRI based measurements with flow-cell system (Wark et al., 2005). Furthermore, if fitting the surface coverage with three different target concentrations (5 nM, 10 nM, and 1 μM of cD1) to the Langmuir adsorption isotherm: $\theta = K_A C/(1 + K_A C)$, a value of $1.72 \times 10^{-8}$ M is obtained for $K_D$ ( = $1/K_A$) which is consistent with the value obtained from kinetic data (Fig. 11, supporting material).

## 4. Conclusions

The optimum mixing frequencies were determined for various cavity diameters and configurations of the VCAT micromixer. The lateral coupling of the bubbles can be seen as the solution is pulled into the chamber and mixed uniformly with the use of the VCAT micromixer. Cavitation microstreaming can be applied to various applications as was shown with the use of three different types of biomolecules including DNA, protein, and modified gold nanoparticles which have different sizes and diffusion coefficients, and can also be applied to microarrays which shows a promising result on biosensing research. The micromixer is able to reduce the time of binding saturation more than a hundred times by overcoming diffusion barriers especially with large molecules. The use of an optimum mixing frequency with the corresponding cavity size and spacing and SPRI provides a powerful tool to decrease microassay times dramatically. Compared to conventional flow through devices using SPRI, cavitation microstreaming offers two distinct advantages: rapid binding and reduced reagent consumption. In a flow through device, approximately 500 μL of fluid is required while for a device utilizing cavitation microstreaming, only 1–2 μL of sample fluid is required. This can save considerably on cost if the reagent in question is expensive or if the reagent is limited in quantity.

## Acknowledgments

This work was partially funded by the Micro/nano Fundamentals Focus (MF3) Center under the DARPA N/MEMS Science and Technology Fundamentals Program, grant no. N66001-10-1-400.

## Appendix A. Supplementary data

Supplementary data associated with this article can be found, in the online version, at doi:10.1016/j.bios.2012.01.028.

## References

Ahmed, D., Mao, X.L., Shi, J.J., Juluri, B.K., Huang, T.J., 2009. Lab on a Chip 9 (18), 2738–2741.
Carrascosa, L., Calle, A., Lechuga, L., 2009. Analytical and Bioanalytical Chemistry 393 (4), 1173–1182.
Chen, Y.L., Nguyen, A., Niu, L.F., Corn, R.M., 2009. Langmuir 25 (9), 5054–5060.
Duffy, D.C., McDonald, J.C., Schueller, O.J.A., Whitesides, G.M., 1998. Analytical Chemistry 70 (23), 4974–4984.
Elder, S.A., 1959. Journal of the Acoustical Society of America 31 (1), 54–64.
Feriotto, G., Ferlini, A., Ravani, A., Calzolari, E., Mischiati, C., Bianchi, N., Gambari, R., 2001. Human Mutation 18 (1), 70–81.
Frietas, R.A.J., 2003. Nanomedicine, vol IIA: Biocompatibility. Landes Biosciences, Georgetown, TX.
Halpern, A.R., Chen, Y., Corn, R.M., Kim, D., 2011. Analytical Chemistry 83 (7), 2801–2806.
He, L., Musick, M.D., Nicewarner, S.R., Salinas, F.G., Benkovic, S.J., Natan, M.J., Keating, C.D., 2000. Journal of the American Chemical Society 122 (38), 9071–9077.
Henares, T.G., Mizutani, F., Hisamoto, H., 2008. Analytica Chimica Acta 611 (1), 17–30.
Hickel, W., Kamp, D., Knoll, W., 1989. Nature 339 (6221), 186.
Jensen, K.K., Ørum, H., Nielsen, P.E., Nordén, B., 1997. Biochemistry 36 (16), 5072–5077.
Lai, S., Wang, S.N., Luo, J., Lee, L.J., Yang, S.T., Madou, M.J., 2004. Analytical Chemistry 76 (7), 1832–1837.
Lee, H.J., Wark, A.W., Corn, R.M., 2006. Langmuir 22 (12), 5241–5250.
Lee, H.J., Wark, A.W., Corn, R.M., 2008. Analyst 133 (5), 596–601.
Liu, R.H., Lenigk, R., Druyor-Sanchez, R.L., Yang, J.N., Grodzinski, P., 2003. Analytical Chemistry 75 (8), 1911–1917.
Liu, R.H., Yang, J.N., Pindera, M.Z., Athavale, M., Grodzinski, P., 2002. Lab on a Chip 2 (3), 151–157.
Lukacs, G.L., Haggie, P., Seksek, O., Lechardeur, D., Freedman, N., Verkman, A.S., 2000. Journal of Biological Chemistry 275 (3), 1625–1629.
Marmottant, P., Hilgenfeldt, S., 2003. Nature 423 (6936), 153–156.
Nelson, B.P., Grimsrud, T.E., Liles, M.R., Goodman, R.M., Corn, R.M., 2000. Analytical Chemistry 73 (1), 1–7.
Nguyen, N.T., Wu, Z.G., 2005. Journal of Micromechanics and Microengineering 15 (2), R1–R16.
Nilsson, P., Persson, B., Larsson, A., Uhlén, M., Nygren, P.A., 1997. Journal of Molecular Recognition 10 (1), 7–17.
Nkodo, A.E., Garnier, J.M., Tinland, B., Ren, H., Desruisseaux, C., McCormick, L.C., Drouin, G., Slater, G.W., 2001. Electrophoresis 22 (12), 2424–2432.
Phillips, K.S., Wilkop, T., Wu, J.J., Al-Kaysi, R.O., Cheng, Q., 2006. Journal of American Chemical Society 128 (30), 9590–9591.
Renaudin, A., Chabot, V., Grondin, E., Aimez, V., Charette, P.G., 2010. Lab on a Chip 10 (1), 111–115.
Reuter, M., Schneider-Mergener, D., Kupper, D., Meisel, A., Mackeldanz, P., Kruger, D.H., Schroeder, C., 1999. Journal of Biological Chemistry 274 (8), 5213–5221.
Rossier, J.S., Gokulrangan, G., Girault, H.H., Svojanovsky, S., Wilson, G.S., 2000. Langmuir 16 (22), 8489–8494.
Rothenhausler, B., Knoll, W., 1988. Nature 332 (6165), 615–617.
Rudyak, V.Y., Dubtsov, S.N., Baklanov, A.M., 2008. Technical Physics Letters 34 (6), 519–521.
Sendroiu, I.E., Corn, R.M., 2008. Biointerphases 3 (3), FD23–FD29.
Shumaker-Parry, J.S., Campbell, C.T., 2004. Analytical Chemistry 76 (4), 907–917.
Stone, H.A., Stroock, A.D., Ajdari, A., 2004. Annual Review of Fluid Mechanics 36, 381–411.
Stroock, A.D., Dertinger, S.K.W., Ajdari, A., Mezic, I., Stone, H.A., Whitesides, G.M., 2002. Science 295 (5555), 647–651.
Tho, P., Manasseh, R., Ooi, A., 2007. Journal of Fluid Mechanics 576, 191–233.
Tovar, A.R., Lee, A.P., 2009. Lab on a Chip 9 (1), 41–43.
Turkevich, J., Stevenson, P.C., Hillier, J., 1951. Discussions of the Faraday Society 11, 55–75.
Wark, A.W., 2008. Handbook of Surface Plasmon Resonance, pp. 251–280.
Wark, A.W., Lee, H.J., Corn, R.M., 2005. Analytical Chemistry 77 (13), 3904–3907.
Wegner, G.J., Wark, A.W., Lee, H.J., Codner, E., Saeki, T., Fang, S.P., Corn, R.M., 2004. Analytical Chemistry 76 (19), 5677–5684.
Wolf, L.K., Fullenkamp, D.E., Georgiadis, R.M., 2005. Journal of American Chemical Society 127 (49), 17453–17459.
Yeatman, E., Ash, E.A., 1987. Electronics Letters 23 (20), 1091–1092.
Zhang, C.S., Xing, D., Li, Y.Y., 2007. Biotechnology Advances 25 (5), 483–514.
Zuker, M., 2003. Nucleic Acids Research 31 (13), 3406–3415.